Latin American Journal of Solids and Structures
www.lajss.org

On the Decreasing Flexural Modulus of Glass/Vinylester Composite Beams Up to Failure State

Abstract

The comparison of the failure state for composite laminates under bending and tensile loads is a well-known issue which has been intensively discussed in the literature. The scope of the current work is to investigate the appropriate method of the flexural modulus of the composite laminates by the aid of experimental and numerical approach. The primary objective of this study is to compare the experimental measurements of the elastic modulus of the composite laminates under the tensile and flexural tests. The numerical study is performed through progressive damage analysis (PDA) approach which is verified by simulation of the tensile specimens. This procedure is then used to predict the failure of the beam specimens under three-point-bending (3PB) test. Both inter-laminar and intra-laminar damages are included in the developed models. The first type of damage is examined based on the continuum damage mechanics (CDM) approach and the second one based on the virtual crack closure technique (VCCT). The variation of the flexural modulus and ultimate strength of the composite beams is considerably depends on loading types and lay-up configurations. In this study, it is proven that the strain-based failure criterion can predict the realistic failure mode of the composite beams in consistency with the ultimate strains which was obtained from a simple tensile test.

Keywords

Flexural strength; Flexural modulus; Glass/Vinylester laminates; Progressive damage; Three-point-bending.

A. R. Nazari [a]
M. Z. Kabir [b, *]
H. Hosseini-Toudeshky [c]

[a] Department of Civil and Environmental Engineering, Amirkabir University of Technology, Tehran, Iran,
E-mail: arnazari@aut.ac.ir
[b] Department of Civil and Environmental Engineering, Amirkabir University of Technology, Tehran, Iran,
E-mail: mzkabir@aut.ac.ir
[c] Department of Aerospace Engineering, Amirkabir University of Technology, Tehran, Iran, E-mail: Hosseini@aut.ac.ir

* Corresponding author

http://dx.doi.org/10.1590/1679-78253662

Received 04.01.2017
In revised form 06.05.2017
Accepted 31.05.2017
Available online 17.06.2017

1 INTRODUCTION

In the last decades, application of fiber reinforced polymer composites has remarkably increased in the infrastructures under various loading conditions (Jones, 1999). Composite materials are usually employed for the numerous kinds of loading such as in-plane and out-of-plane situations. As the mechanical properties of the polymeric materials appear to be variable under various loading types, numerous researchers attempted to explain this phenomenon on the fiber reinforced polymers. The existing papers indicate that in some cases considerable differences have been detected between the mechanical properties of the composite laminates measured under bending and tensile loads. The ultimate flexural strength is reported generally larger than the tensile strength. This subject has an old background in the literature. Bullock (1974) reported the ratio of strengths between 3PB and tensile loadings of 1.35 and 1.49 for two types of graphite-epoxy composites. Whitney and Knight (1980) measured this ratio as 1.04 to 1.33 for the graphite-epoxy laminates. Weibull theory (Bullock, 1974) predicts a higher strength for material under bending load than its tensile strength since it assumes that the strength of materials is affected by some critical defects which are distributed statistically in the material. Cattell and Kibble (2001) examined 3PB beams with the span-to-depth ratio (L/D) of 20 and measured the ratio of flexural to tensile strength equal to 1.4. They tried to predict this ratio using Weibull theory. Ullah et al. (2012) reported the flexural strength of the woven fabric CFRP laminates under bending load of 10% larger than the tensile strength. Although there are some researches which show that prediction of the flexural strength using Weibull theory often produces satisfactory results, sometimes large discrepancies have been reported between the results predicted by this theory and the experimental results (Wisnom, 1992).

For the polymeric materials, two different moduli are determined as the tensile and flexural moduli that the first parameter is measured based on the tensile stress-strain curve and the second one is calculated according to the load-deflection curves from the bending tests. Jones (1978) derived the elastic moduli of various composite materials under tension, compression, 3PB (three-point bending) and 4PB (four-point bending) conditions and deduced that no clear pattern of larger tension than compression modulus or vice versa exists for these materials. Zweben (1994) and Smith et al. (1979) introduced the value of the flexural modulus smaller than the tensile modulus for the unidirectional kevlar 49/polyester composite beams. Tolf and Clarin (1984) measured the flexural modulus 11% smaller than the tensile modulus for the E-glass/polyester specimens. Roopa et al. (2014) reported the ratio of flexural to tensile moduli equal to 4 and 2.67 for glass/polyester and glass/vinyl ester specimens, respectively. The complexity of the flexural behavior of the polymeric materials is understood when it is considered that the flexural properties vary with specimen depth, temperature and rate of straining (loading) (ASTM D790–07, 2007). There are some investigations in the literature indicating that the main cause of inconsistency between the flexural and tensile moduli in the composite laminates is related to the difference between the compressive and tensile moduli of the materials. By consideration of a lower compressive modulus than the tensile modulus for carbon/epoxy laminates, Mujika et al. (2006) and Moreno et al. (2015) estimated a lower flexural modulus for these composite laminates than the tensile modulus. Of course, this reason is not the only factor for difference of the flexural and the tensile moduli. For example the flexural modulus is not a constant value and changes for various L/D ratios of the beams, however, both the tensile and the compressive moduli are constant values. In the FRP materials, the fibers have usually linear

elastic behavior and the polymeric matrix is subjected to nonlinear behavior due to the occurrence of damage and plasticity. Variation of the mechanical properties under different loading conditions is also attributed to the nonlinear behavior of the polymeric part of the composite materials. For the composite laminates made of high modulus fibers, a lower difference is usually expected between the flexural and the tensile moduli as reported in the literature and also a higher difference is expected for the composite laminates made of vinyl ester and polyester resins in comparison to the laminates made of epoxy resin.

For the sake of accurate investigation of the mechanical properties of the composite laminates up to the failure state, taking into account of the influence of the various damage modes on the material behavior is an essential task. The damage of the composite laminates is usually initiated by matrix cracking and delamination modes which degrade the stiffness of the laminates prior to the ultimate strength. So a more accurate simulation of the load carrying of the composite laminates under bending is accomplished using progressive damage analysis (PDA). By considering of material nonlinearity and more accurate simulation of the boundary conditions, the presented results in the recent researches are more accurate than those, obtained by the earlier numerical researches (Echaabi et al., 1996; Smith and Ogin, 1999). Of course, PDA of the composite laminates has a great background in the literature. Ochoa and Reddy (1992) presented a comprehensive review of the basic steps for performing progressive failure analysis. Garnich and Akula (2009) reviewed a brief summary of the major classes of failure criteria pertaining to the degradation models. Generally, the progressive damage studies investigate two main stages as (i) initiation of damage in various damage modes which are characterized by interactive or non-interactive failure criteria and, (ii) evolution of damage in each mode to accomplish complete failure. Soden et al. (1998) and Soden et al. (1998) presented a comprehensive comparison between the predictions of recognized failure theories for fiber-reinforced composite laminates. The strain-based and energy-based failure criteria produce more reliable results for composite components under multi-axial stresses or bending conditions than the results obtained by the stress-based criteria (Wolfe and Butalia, 1998; Mines and Alias, 2002; Doudican et al. 2012; Meng et al. 2015). Also, the interlaminar failure is examined by cohesive elements and virtual crack closure techniques. Of course, recent advances of various FE codes have provided a unique opportunity for researchers to implement more accurate analyses with considering of damage effects on the performance of the composite laminates (Lade`veze and Lubineau, 2002; Sadeghi et al. 2014).

In this paper, the load carrying capacity of the glass/vinyl ester composite laminates was examined under 3PB flexural loading conditions up to the failure state. The variation of the bending modulus and ultimate stress under various loading is examined for the various layups configuration of the laminates by the experimental and FE simulation. The experimental program includes tensile tests to verify the developed PDA procedure for composite laminates. Then, the objective of the paper is followed by examining 3PB laminate beams with various layups comprising of 0° and 90°-plies. For a description of the material response, the experimental specimens are simulated by the nonlinear FE analysis. The flexural failure of the glass/vinyl ester composite beams was observed different with the failure of the carbon/epoxy laminates, addressed in the literature. The reason for the difference between the flexural and tensile modulus was attributed to the different response of the 90°-plies on the laminates under tensile and flexural loads. The progressive failure analyses are

performed on the composite beams by considering the intralaminar damage modes based on the CDM approach and the interlaminar damage using VCCT. By considering the various damage modes and nonlinear behavior for the contact of the specimens and supports, the FE model achieves to accurate results about the mechanical properties of the laminates. To predict the intralaminar failure, the strain-based failure criteria are implemented in the developed subroutine, linked to ABAQUS software. It is shown that the developed FE models estimate the flexural moduli of the composite laminates for various layups, accurately. The strain-based failure criteria on the basis of the ultimate strains, measured for the tensile specimens, can predict the failure load of the composite beams with acceptable accuracy.

2 EXPERIMENTS

The density and tensile strength of the fibers sheet implemented for the production of the specimens were considered as 400 gr/m^2 and 600 MPa, respectively. The laminates composed of 0° and 90°-plies. The resin was a vinyl ester with the nominal tensile strength of 30 MPa. Three layup methods were employed for fabrication of the laminate plates using compact molding technique. The fiber volume fraction was considered around 65%. The laminates were cured at a temperature of $60^\circ C$ for the duration of 48 hours. In the exterior side of the laminates, a blue color coating gel with a thickness of 0.1 mm was applied to protect the specimens from weathering, moisture and chemical exposure. Table 1 shows the mechanical properties of the produced GFRP layers, obtained from the standard characterization tests (Nazari, 2016). The tensile and 3PB experiments were conducted at the room temperature when the laminates density was 1800 kg/m^3. The tensile test setup is presented in Figure 1. Two strain gages were attached to each specimen: one in the longitudinal and the other in the transverse direction to measure the Poisson ratio of the laminates. All experiments were conducted by a ZWICK machine under displacement controlled loading conditions when the crosshead velocity of the servo-hydraulic testing machine was 1 mm/min. The load was measured by the machine load cell and the mid-span deflection for the composite beams under flexural test was measured equal to the displacement of the cross-head. Zweben (1994) and Smith et al. (1979) recommended the L/D (span to length) ratio of 60 and 16 for measuring the flexural modulus and the ultimate strength of the composite beams, respectively. ASTM D790–07 (2007) recommends L/D ratio of 32 for highly orthotropic laminates. Therefore, in this study, two L/D ratios were applied for 3PB tests as 67 (large span) and 33 (small span). The dimensions and layups of the beam specimens are listed in Table 2. Three coupons for each specimen were tested to assure the consistency of the experimental results and the average data were depicted. In this table ST represents the tensile specimen and SF stands for the flexural specimens.

Properties	E_1 (MPa)	E_2 (MPa)	E_3 (MPa)	ν_{12}	ν_{13}	ν_{23}	G_{12} (MPa)	G_{13} (MPa)	G_{23} (MPa)
Glass/Vinylester	11900	1350	1350	0.2	0.2	0.35	1070	770	770

Table 1: The Mechanical properties of the UD GFRP laminas (Nazari, 2016)

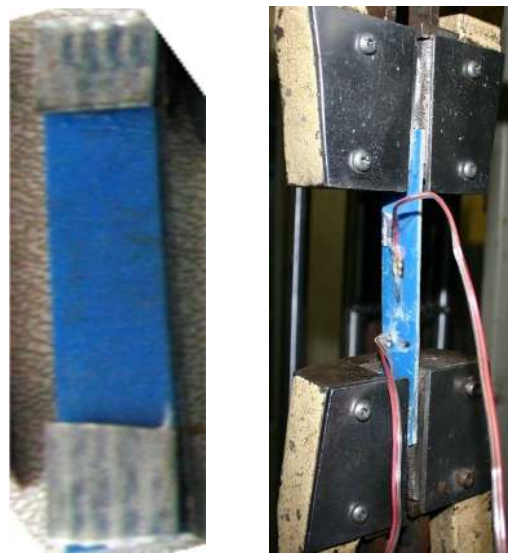

Figure 1: Test setup for the tensile specimens.

Specimen	L_1	L_2	W	D	Layup
ST-1	100	151	20	4×0.75	$(0)_4$
ST-2	100	153	19.5	4×0.75	$(90)_4$
ST-3	100	153	19.6	4×0.75	$(90,0_3)$
ST-4	100	152	20.3	4×0.75	$(0,90_3)$
ST-5	100	149.5	19.5	4×0.75	(0,90,0,90)
ST-6	100	148	20.3	4×0.75	(90,0,90,0)
SF-1	200	255	50.5	4×0.75	$(0)_4$
SF-2	100	150.5	19.5	4×0.75	$(0)_4$
SF-3	100	151	19.5	4×0.75	$(90)_4$
SF-4	100	151	20.7	4×0.75	$(90,0_3)$
SF-5	100	152	19.6	4×0.75	$(0,90_3)$
SF-6	100	150.5	20.3	4×0.75	(0,90,0,90)
SF-7	100	150.3	20.3	4×0.75	(90,0,90,0)

Table 2: Dimensions and layup of the experimental specimens according to the geometry presented in Figure 2.

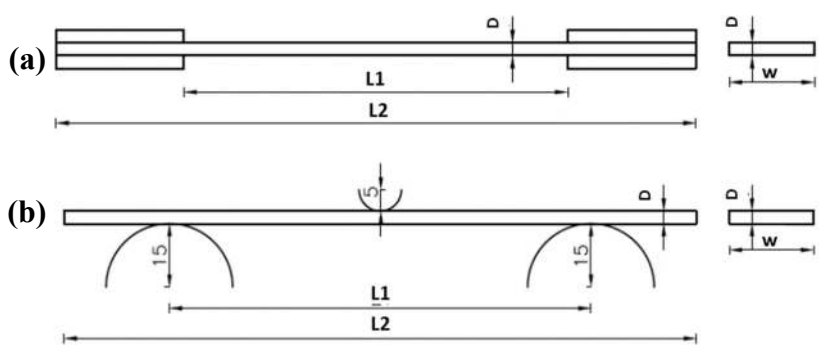

Figure 2: Geometrical parameters of the (a) tensile and (b) flexural specimens.

Table 3 shows the results of the various coupons for each specimen, examined in the experiments. The results, addressed in the other sections of this paper, indicate the mean value of the results obtained by various coupons for each specimen. Figure 3(a) shows SF-2 beam specimen under loading and Figure 3(b) shows failure mode of the SF-2 specimen. Based on the elementary mechanics of materials the flexural modulus of 3PB beams is calculated by (ASTM D790–07; 2007):

$$E_B = L^3 m / 4bd^3 \tag{1}$$

where E_B is the modulus of elasticity in bending, L is the support span, b and d are the widths and the depth of the beam specimen, respectively and m is the slope of the tangent to the initial straight-line segment of the load-deflection curve. ASTM D790 denote that Equation (1) produces reliable results for small deflections when $(dw/dx)^2$ is noticeably small compared to unity (Timoshenko and Gere, 1972). The large deflection of the composite beams, examined in this study, showed that the obtained result by this formula will not accomplish a reasonable accuracy, however, there is no other standard code to be referred for determination of the flexural modulus in the composite beams with large deflections. Of course, Equation (1) can achieve an approximate value from the real flexural modulus of the composite beams. The stress at the outer surface of the beam specimen is estimated by (ASTM D790–07; 2007):

$$\sigma_f = (3PL/2bd^2)[1+6(D/L)^2 - 4(d/L)(D/L)] \tag{2}$$

where σ_f is the stress in the outer fibers at the midpoint, P is the load at a given point on the load-deflection curve, D is a deflection of the centerline of the specimen at the middle of the support span. ASTM implies that the accuracy of the results obtained by Equations (1) and (2) will decrease if the beam specimen slips excessively between the supports due to large deflections.

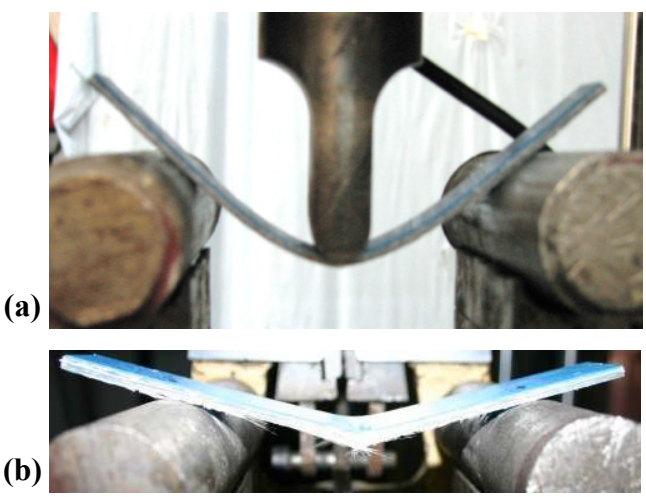

Figure 3: (a) SF-2 specimen under 3PB test; (b) Failure of SF-2 specimen by rupture of the tensile fibers.

Tensile specimens	Maximum stress (MPa)	Mean value (MPa)	Standard deviation (MPa)	Elastic modulus (Mpa)	Mean value (MPa)	Standard deviation (MPa)	Flexural specimens	Maximum load (N)	Mean value (MPa)	Standard deviation (MPa)	Maximum deflection (mm)	Mean value (N)	Standard deviation (N)
	331.72			11,826				112.32			12.10		
ST-1	335.55	329.92	6.71	11,807	11,822	13	SF-1	111.22	113.03	2.25	11.60	12.25	0.74
	322.50			11,833				115.54			13.05		
	39.18			1,338				634.70			20.51		
ST-2	36.23	38.18	1.69	1,327	1,335	7	SF-2	622.05	637.02	16.25	21.12	22.14	2.31
	39.12			1,341				654.30			24.78		
	264.14			11,235				153.80			21.43		
ST-3	274.45	263.82	10.79	11,195	11,236	41	SF-3	150.20	154.44	4.59	18.21	20.61	2.12
	252.87			11,276				159.32			22.20		
	110.87			4,146				359.00			22.90		
ST-4	119.23	111.85	6.94	4,125	4,165	52	SF-4	349.80	356.53	5.89	23.35	24.71	2.75
	105.45			4,223				360.78			27.87		
	191.33			11,471				106.26			13.72		
ST-5	177.34	190.26	12.41	11,433	11,441	27	SF-5	102.32	105.31	2.64	12.21	13.45	1.13
	202.10			11,420				107.34			14.41		
	189.32			11,511				323.81			20.94		
ST-6	188.23	192.96	7.27	11,534	11,570	83	SF-6	318.98	324.48	5.86	21.70	22.38	1.87
	201.34			11,665				330.65			24.50		
								312.54			19.71		
-	-	-	-	-	-	-	SF-7	312.98	316.65	6.74	16.78	18.97	1.93
								324.43			20.43		

Table 3: The results of three coupons, obtained for various specimens in the experimental program.

3 FINITE ELEMENTS MODELING

Finite elements (FE) simulations of the experimental specimens were carried out using ABAQUS software. The composite laminates were modeled using eight-node solid elements while the supports and the loading head were simulated by rigid shell elements. For simulation of the tensile tests, fixed boundary conditions were applied to the end plates. The axial load was applied by considering a velocity load on the top rigid plate when the bottom rigid plate was considered to be fixed. The degrees of freedom (DOFs) at two ends of the specimens were constrained to the DOFs of the rigid plates using "Tie" interaction in ABAQUS. Half of the beam span was modeled due to the symmetry conditions of the 3PB specimens, while the appropriate boundary conditions were employed on the symmetry surface. The contact between the specimen and the supports was defined in both normal and tangential directions with a proper friction coefficient to control slippage of the specimens on the supports during the loading state. By physical evaluation of the contact surfaces, the friction coefficient between the rollers and the specimens was assumed to be μ=0.3. Batra et al. (2012) assumed this coefficient as μ=0.25 for simulation of the contact between the composite beams and metallic supports. The mesh convergence study showed that discretizing the thickness of the UD laminates by one element per layer produces a sufficient accuracy but in the laminates with different orientation of the adjacent layers, each layer must be discretized by at minimum two elements. At the mid-span area, the beams were meshed by smaller elements because larger deformation gradient is seen in this area.

Both inter-laminar and intralaminar damage modes were included in the FE models. The intralaminar damage was modeled based on the CDM theory while the inter-laminar (delamination) damage was modeled using Virtual Crack Closure Technique (VCCT). Based on the CDM concept, at each integration point of the elements, a framework which accounts for the stiffness degradation of the material was employed. For this purpose, VUSDFLD subroutine, predetermined by ABAQUS, was developed and linked to the main program. This subroutine determines the material mechanical properties dependent of some updating damage variables. Delamination was simulated by definition of a contact interaction between the various layers of the laminates where may be debonded due to excessive inter-laminar stresses. The explicit dynamic technique was employed for numerical progressive damage analyses.

3.1 Intra-Laminar Damage Model

Based on the CDM theory, the damaged state of the material is related to its intact state by implementing damage variables in order to degrade the mechanical properties. The ABAQUS software (2010) proposes a PDA model for 2D elements based on the cohesive constitutive model of Camanho and Davila (2002) in combination with the Hashin damage initiation criteria (Hashin, 1965; Hashin and Rotem, 1973). In this study, the same procedure was extended by a user subroutine (VUSDFLD) to implement PDA on the 3D elements.

The first subject for investigation of the progressive damage in the composite laminates is a determination of the damage initiation state using well-known failure criteria. Degradation of the elements' stiffness is activated by initiation in one failure mode and then growths through the damage variables. The accuracy of the various failure criteria may depend on the type of the composite material, structural configuration and loading conditions. Sometimes prediction of the flexural failure using the stress-based criteria may be followed by considerable errors so, in this research, initiation and progression of damages in various modes are predicted using strain-based criteria. These criteria are associated with the Hashin failure theory, however, regarding the difference between the maximum stress measured under bending and tensile loads, they are calculated based on the strain components. The considered intralaminar damage modes are as:

- Fibers rupture in tension (f_1);
- Fibers buckling and kinking in compression (f_2);
- Matrix cracking under transverse tension and shearing in local 2 and 3 directions (f_3); and
- Matrix crushing under transverse compression and shearing in local 2 and 3 directions (f_4);

On the basis of these damage modes, four damage criteria are introduced to check damage probability when they are violated as (Hashin and Rotem, 1973):

$$f_1 = \left(\frac{\varepsilon_{11}}{\varepsilon_f^t}\right)^2 + \frac{\varepsilon_{12}^2 + \varepsilon_{13}^2}{\left(\varepsilon_l^s\right)^2} \le 1 \qquad (\varepsilon_{11} \ge 0) \tag{3}$$

$$f_2 = \left(\frac{\varepsilon_{11}}{\varepsilon_f^c}\right)^2 \le 1 \qquad (\varepsilon_{11} < 0) \tag{4}$$

$$f_3 = \left(\frac{\varepsilon_{22} + \varepsilon_{33}}{\varepsilon_m^t}\right)^2 + \frac{\varepsilon_{12}^2 + \varepsilon_{13}^2}{\left(\varepsilon_l^s\right)^2} + \left(\frac{1}{\left(\varepsilon_t^s\right)^2}\right)\left(\varepsilon_{23}^2 - \varepsilon_{22}\varepsilon_{33}\right) \le 1 \qquad (\varepsilon_{22} + \varepsilon_{33} \ge 0) \tag{5}$$

$$f_4 = (\frac{\varepsilon_{22} + \varepsilon_{33}}{2\varepsilon_l^s})^2 + (\frac{\varepsilon_{22} + \varepsilon_{33}}{\varepsilon_m^c})\left[(\frac{\varepsilon_m^c}{2\varepsilon_t^s})^2 - 1\right] + (\frac{\varepsilon_{12}^2 + \varepsilon_{13}^2}{(\varepsilon_l^s)^2}) + (\frac{\varepsilon_{23}^2 - \varepsilon_{22}\varepsilon_{33}}{(\varepsilon_t^s)^2}) \le 1 \qquad (\varepsilon_{22} + \varepsilon_{33} < 0) \tag{6}$$

where ϵ_{ij} are the strain components in 3D elements, ϵ_f^t and ϵ_m^t are the tensile failure initiation strains in fibers and transverse directions, respectively, ϵ_f^c and ϵ_m^c are the compressive failure initiation strains in fibers and transverse directions, respectively, ϵ_l^s is the shear failure initiation strain in the fiber and transverse planes (1-2 and 1-3) and ϵ_t^s is the shear failure initiation strain in the transverse and normal plane (2-3). The abovementioned criteria include the effects of 3D stresses through the Poisson effect. The effective stresses on the damaged elements are obtained by:

$$\hat{\boldsymbol{\sigma}} = \mathbf{M}\,\boldsymbol{\sigma} \tag{7}$$

where M is the diagonal matrix of the damage operators as [Lapczyk and Hurtado, 2007]:

$$\mathbf{M} = \begin{bmatrix} 1/(1-d_f) & 0 & 0 & 0 & 0 & 0 \\ 0 & 1/(1-d_m) & 0 & 0 & 0 & 0 \\ 0 & 0 & 1/(1-d_m) & 0 & 0 & 0 \\ 0 & 0 & 0 & 1/(1-d_l^s) & 0 & 0 \\ 0 & 0 & 0 & 0 & 1/(1-d_l^s) & 0 \\ 0 & 0 & 0 & 0 & 0 & 1/(1-d_t^s) \end{bmatrix} \tag{8}$$

where, d_f, d_m, d_l^s and d_t^s are damage variables associated with fibers, matrix, shear damage in the fiber and transverse planes, and shear damage in the transverse and normal plane, respectively. Since the majority of the composite laminates have different failure mechanisms under tensile and compressive loads, d_f and d_m are distinguished by t and c subscripts for tension and compression performances as (Lapczyk and Hurtado, 2007):

$$d_f = \begin{cases} d_f^t & if\ \varepsilon_{11} \ge 0 \\ d_f^c & if\ \varepsilon_{11} < 0 \end{cases} \tag{9}$$

$$d_m = \begin{cases} d_m^t & if\ \ (\varepsilon_{22} + \varepsilon_{33}) \ge 0 \\ d_m^c & if\ \ (\varepsilon_{22} + \varepsilon_{33}) < 0 \end{cases} \tag{10}$$

$$d_l^s = 1 - (1-d_f^t)(1-d_f^c)(1-d_m^t)(1-d_m^c) \tag{11}$$

$$d_t^s = 1 - (1-d_m^t)^2 (1-d_m^c)^2 \tag{12}$$

The damage evolution is established based on the progression of the complementary free energy density in the material which is determined as (Maimi et al., 2007):

$$\begin{aligned} G = {} & \frac{1}{2E_1}(\frac{\langle\sigma_{11}\rangle^2}{1-d_f^t} + \frac{\langle-\sigma_{11}\rangle^2}{1-d_f^t}) + \frac{1}{2E_2}(\frac{\langle\sigma_{22}\rangle^2}{1-d_m^t} + \frac{\langle-\sigma_{22}\rangle^2}{1-d_m^c}) + \frac{1}{2E_3}(\frac{\langle\sigma_{33}\rangle^2}{1-d_m^t} + \frac{\langle-\sigma_{33}\rangle^2}{1-d_m^c}) \\ & - \frac{\nu_{12}\sigma_{11}\sigma_{22}}{E_1} - \frac{\nu_{13}\sigma_{11}\sigma_{33}}{E_1} - \frac{\nu_{23}\sigma_{22}\sigma_{33}}{E_2} + \frac{\sigma_{12}^2}{G_{12}(1-d_l^s)} + \frac{\sigma_{13}^2}{G_{13}(1-d_l^s)} + \frac{\sigma_{23}^2}{G_{23}(1-d_t^s)} \end{aligned} \tag{13}$$

where the operator of "<>" is Macaulay bracket, defined for every ωϵR as <ω>= (ω+|ω|)/2. To ensure the irreversibility of the damage process, the rate of change of the complementary free energy Ġ minus the externally supplied work to the solid at constant strains, $\dot{\boldsymbol{\sigma}}:\boldsymbol{\varepsilon}$, must be non-negative:

$$\dot{\mathbf{G}} - \dot{\boldsymbol{\sigma}} : \boldsymbol{\varepsilon} \geq 0 \tag{14}$$

and expanding the inequality in terms of the stress tensor and the damage variables gives (Maimi et al., 2007):

$$\left(\frac{\partial \mathbf{G}}{\partial \sigma} - \varepsilon\right) : \dot{\boldsymbol{\sigma}} + \frac{\partial \mathbf{G}}{\partial d_f}\dot{d}_f + \frac{\partial \mathbf{G}}{\partial d_m}\dot{d}_m + \frac{\partial \mathbf{G}}{\partial d_l}\dot{d}_l^s + \frac{\partial \mathbf{G}}{\partial d_t}\dot{d}_t^s \geq 0 \tag{15}$$

Since the stresses are variables, the expression in the parenthesis must be equal to zero to ensure positive dissipation of the energy (Maimi et al., 2007):

$$\boldsymbol{\varepsilon} = \frac{\partial \mathbf{G}}{\partial \boldsymbol{\sigma}} = \mathbf{H} : \boldsymbol{\sigma} \tag{16}$$

$$\boldsymbol{\sigma} = \mathbf{C}_d \boldsymbol{\varepsilon} \tag{17}$$

H is the flexibility matrix and $\mathbf{C}_d$ is the stiffness matrix of the damaged element. Using the above relation and the quantitative assessments for degradation of the Poisson ratio, the components of the degraded stiffness matrix are obtained as presented in App. A. By separating the influential terms of the complementary free energy about the various modes of failure, an equivalent energy (G_{eq}) for each mentioned mode is established for investigation of the damage evolution in the elements. Since the dissipated energy is proportional to the volume of the elements, it varies with mesh refinement so the equivalent energies (G_{eq}s) are normalized regarding a characteristic length for the elements, L_c, which is defined by Bazant and Oh (1983) for brick elements as:

$$L^C = \sqrt[3]{V_{el}} \tag{18}$$

where V_{el} is the volume of the elements. The equivalent energy is defined as the area under the curve of equivalent stress versus equivalent displacement for various failure modes (see Figure 4) as:

$$\begin{aligned} \delta_{f,eq}^t &= L^C \sqrt{\langle \varepsilon_{11} \rangle^2 + \varepsilon_{12}^2 + \varepsilon_{13}^2} \\ \sigma_{f,eq}^t &= \frac{\langle \sigma_{11} \rangle \langle \varepsilon_{11} \rangle + \tau_{12}\varepsilon_{12} + \tau_{13}\varepsilon_{13}}{\delta_{eq}^{ft} / L^C} \end{aligned} \tag{19}$$

for fibers in tension $(\sigma_{11} \geq 0)$;

$$\begin{aligned} \delta_{f,eq}^c &= L^C \langle -\varepsilon_{11} \rangle \\ \sigma_{f,eq}^c &= \frac{\langle -\sigma_{11} \rangle \langle -\varepsilon_{11} \rangle}{\delta_{eq}^{ft} / L^C} \end{aligned} \tag{20}$$

For fibers in compression $(\sigma_{11} < 0)$;

$$\delta_{m,eq}^{t} = L^{C}\sqrt{\langle \varepsilon_{22} + \varepsilon_{33} \rangle^{2} + (\varepsilon_{12}^{2} + \varepsilon_{13}^{2})}$$
$$\sigma_{m,eq}^{t} = \frac{\langle \sigma_{22} \rangle \langle \varepsilon_{22} \rangle + \langle \sigma_{33} \rangle \langle \varepsilon_{33} \rangle + \tau_{12}\varepsilon_{12} + \tau_{13}\varepsilon_{13}}{\delta_{eq}^{mt} / L^{C}} \tag{21}$$

For matrix in tension and shear $(\sigma_{22} + \sigma_{33} \geq 0)$; and

$$\delta_{m,eq}^{c} = L^{C}\sqrt{\langle -(\varepsilon_{22} + \varepsilon_{33}) \rangle^{2} + (\varepsilon_{12}^{2} + \varepsilon_{13}^{2})}$$
$$\sigma_{m,eq}^{c} = \frac{\langle -(\sigma_{22} + \sigma_{33}) \rangle \langle -(\varepsilon_{22} + \varepsilon_{33}) \rangle + \tau_{12}\varepsilon_{12} + \tau_{13}\varepsilon_{13}}{\delta_{eq}^{mc} / L^{C}} \tag{22}$$

For matrix in compression $(\sigma_{22} + \sigma_{33} < 0)$. The damage variable associated with each failure mode i, takes values between zero (undamaged state) and one (fully damaged state) as (Maimi et al., 2006):

$$d_{j}^{i} = \frac{(\delta_{j,eq}^{i})^{u}(\delta_{j,eq}^{i} - (\delta_{j,eq}^{i})^{0})}{\delta_{j,eq}^{i}((\delta_{j,eq}^{i})^{u} - (\delta_{j,eq}^{i})^{0})} \qquad i = t,c \quad and \quad j = f,m \tag{23}$$

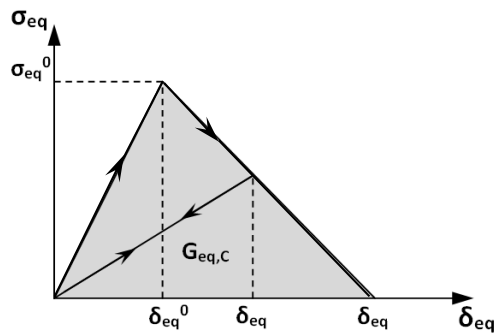

Figure 4: Schematic of equivalent stress versus equivalent displacement diagram (Maimi et al., 2006).

Using Table 4 and those obtained by characterization tests (Nazari, 2016), $(\delta^{i}_{j,eq})^{0}$ are achieved by damage initiation strains, $(\delta^{i}_{j,eq})^{u}$ are obtained by the final failure strains and $\delta^{i}_{j,eq}$ is derived from the available strains in the material after damage initiation. Figure 4 shows that when the values of $\delta^{i}_{j,eq}$ and $\sigma^{i}_{j,eq}$ are determined for a material, the value of equivalent energy (G_{eq}) for each mentioned mode of failure is definite for investigation of the damage evolution in the elements.

3.2 Inter-Laminar Damage (Delamination) Model

Delamination may occur in three modes of inter-laminar failure between the plies as opening, sliding and tearing. Previously, the achieved investigations reported the occurrence of delamination during the flexural failure of the composite beams (Wisnom and Atkinson, 1997) so delamination initiation

and propagation were considered for simulating the ultimate state of the beam specimens using the Virtual Crack Closure Technique (VCCT). The complete explanation of this procedure can be found in the related researches (Rybicki and Kanninen, 1977; Krueger, 2002) and the details are omitted here to keep conciseness. Based on this technique and considering Figure 5, the strain energy release rates (SERRs) for three inter-laminar damage modes are calculated as:

$$G_I = \frac{1}{2\Delta A} F_z^i (u_z^j - u_z^{j^*}) \tag{24}$$

$$G_{II} = \frac{1}{2\Delta A} F_x^i (u_x^j - u_x^{j^*}) \tag{25}$$

$$G_{III} = \frac{1}{2\Delta A} F_y^i (u_y^j - u_y^{j^*}) \tag{26}$$

Where $\Delta A = b.\Delta a$ is the virtually closed crack surface area, Δa is the length of the elements at the delamination front and b is the width of the element. In this procedure, the assumption of a small cracked area between the susceptible layers for delamination is necessary. Therefore, in the FE models, a small delaminated area (with 0.1 mm length) was replaced between the layers of the laminates at the beam mid-span region. Of course, negligibility of the influence of this small delamination on the load carrying capacity of the beams was checked. In order to examine the influence of the mixed-mode delamination, the Power law (Wu and Reuter, 1965) was utilized as:

$$\frac{G_{equiv}}{G_{equivC}} = \left(\frac{G_I}{G_{IC}}\right)^{\alpha_m} + \left(\frac{G_{II}}{G_{IIC}}\right)^{\alpha_n} + \left(\frac{G_{III}}{G_{IIIC}}\right)^{\alpha_0} \tag{27}$$

The introduced parameters in this formula, G_{IC}, G_{IIC}, G_{IIIC}, α_m, α_n and α_0 must be characterized. With acceptable accuracy, α_m, α_n and α_0 have assumed unity since the FE results showed the occurrence of delamination in the beams mainly due to one mode (the influence of other modes was negligible). The critical values of the SERRs between the UD layers of the examined laminates were measured as G_{IC}=0.9 N/mm and G_{IIC}= G_{IIIC}=1.5 N/mm.

Properties	UD Lamina	Properties	UD Lamina
$(\epsilon^t_f)^0$	0.029	$(\epsilon^c_m)^0$	0.002
$(\epsilon^t_f)^u$	0.029	$(\epsilon^c_m)^u$	0.065
$(\epsilon^t_m)^0$	0.0013	$(\epsilon^s_l)^0$	0.0019
$(\epsilon^t_m)^u$	0.0255	$(\epsilon^s_l)^u$	0.037
$(\epsilon^c_f)^0$	0.032	$(\epsilon^s_t)^0$	0.0022
$(\epsilon^c_f)^u$	0.032	$(\epsilon^s_t)^u$	0.043

Table 4: Ultimate strains of the examined GFRP laminas (Nazari, 2016; Nazari et al., 2017).

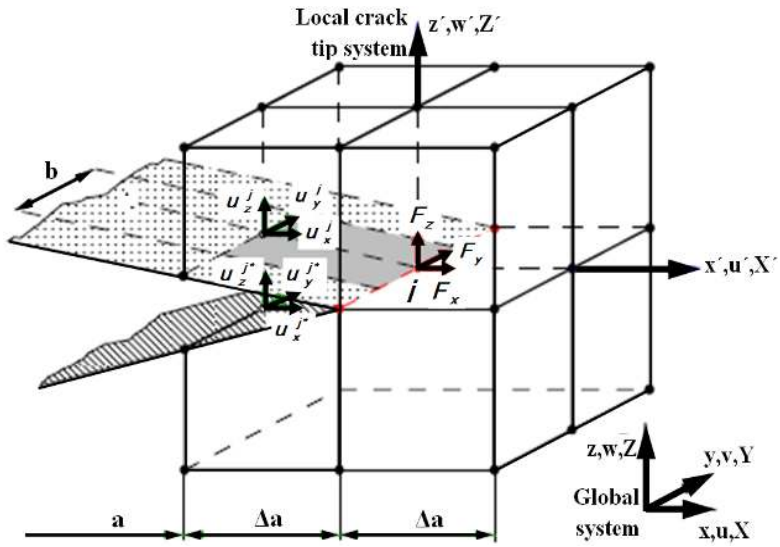

Figure 5: Modified virtual crack closure technique for eight-node solid elements (Rybicki and Kanninen, 1977; Krueger, 2002).

4 DISCUSSIONS OF THE RESULTS

In this section, the developed PDA procedure is verified using the obtained results for the tensile tests. Since the damage evolution rule adopted for simulation of the laminates is assumed to be identical under bending and tensile loads, the variation of the mechanical properties measured for the laminates under the bending and tensile loads is determined based on the FE study.

4.1 Verification of PDA

The stress-strain curves, obtained from experiments and FE models, are shown in Figure 6 for various specimens. Comparison of the presented results in Figure 6 shows a good agreement between the numerical analyses and experimental results. The size of the elements at the surface of the tensile specimens was 5 mm while the thickness of each ply in the laminates was discretized by one element. Figure 7(a) shows the longitudinal stress distribution for the FE model of the ST-1 specimen prior to the failure state. In this figure, the boundary conditions of the tensile models are also observed. Figure 7(b) shows the distribution of the tensile fibers failure criterion at the same state. The FE model shows that the maximum tensile stress occurred in this specimen was achieved around 345 MPa. The difference between the stress measured by the FE model as 345 MPa and the experimental result as 330 MPa is ascribed to the difference of the true and engineering stresses. Figure 6 indicated that the stress-strain curve of the specimen with UD 0°-plies is linear however considerable nonlinearity is observed for the specimen with UD 90°-plies.

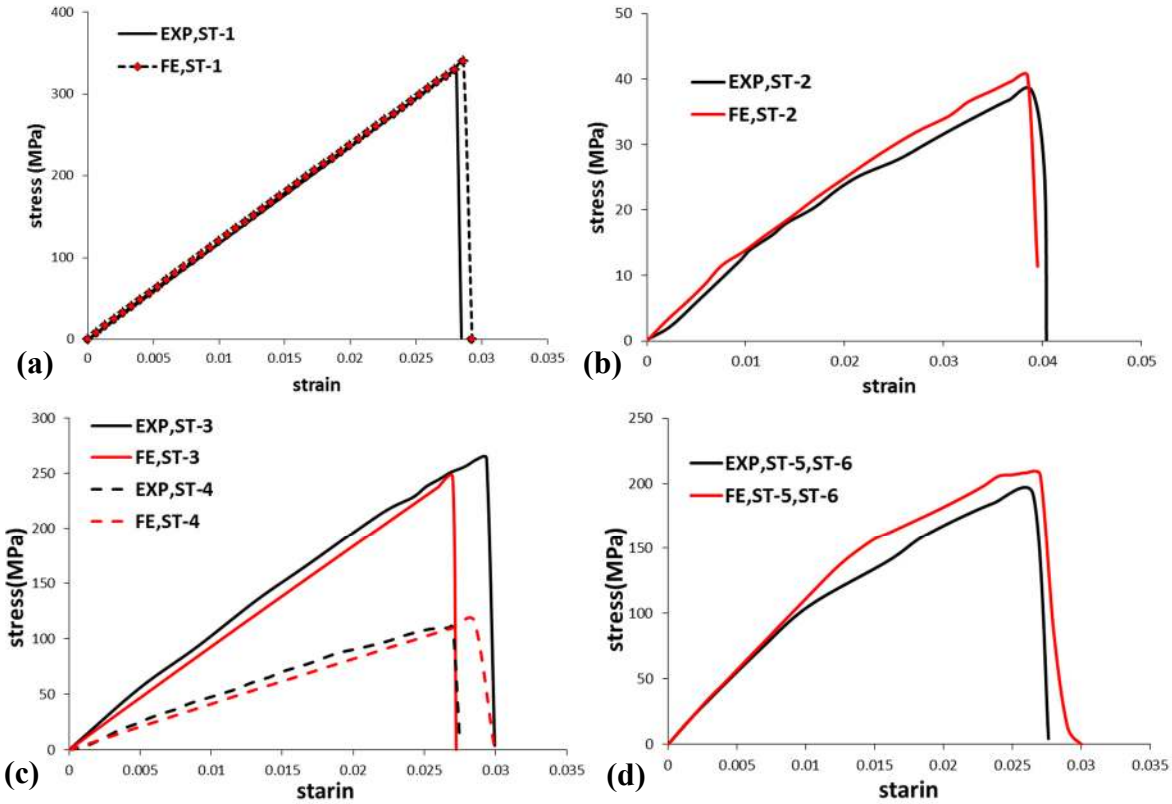

Figure 6: Tensile stress-strain response obtained from experiments and FE models for (a) ST-1, (b) ST-2, (c) ST-3 and ST-4, (d) ST-5 and ST-6 specimens.

4.2 Bending Specimens

4.2.1 UD Laminates

The failure behavior of the various beam laminates with different layup configuration containing 0° and 90°-plies are investigated in this section. The beams with UD 0°-plies were examined for two L/D ratios: 33 and 67. The thickness of the UD beams was discretized by four elements (one element per layer) while the general size of the elements along the length of the beams was 5 mm which decreased to 1 mm close to the mid-span area. The load-deflection curves obtained from the experiment and FE models for SF-1 specimen are shown in Figure 8. In this figure, P and Δ denote the applied load and the mid-span deflection, respectively. No visible macro damages were observed for SF-1 specimen with L/D=67 during the loading state and the FE results also were verified. So the concerned issue for this beam was an inspection of the cause of reduction of the load carrying capacity in the absence of the macro damages in this beam. The FE results for this model showed that due to slippage of the beam at the support positions, resulted in an excessive increase of the beam deflection, the beam bending span was increased which led to a reduction of the load carrying capacity. Variation of the load versus the curved length of the span, L, in Figure 9 shows a significant effect of the beam span length on the load bearing capacity.

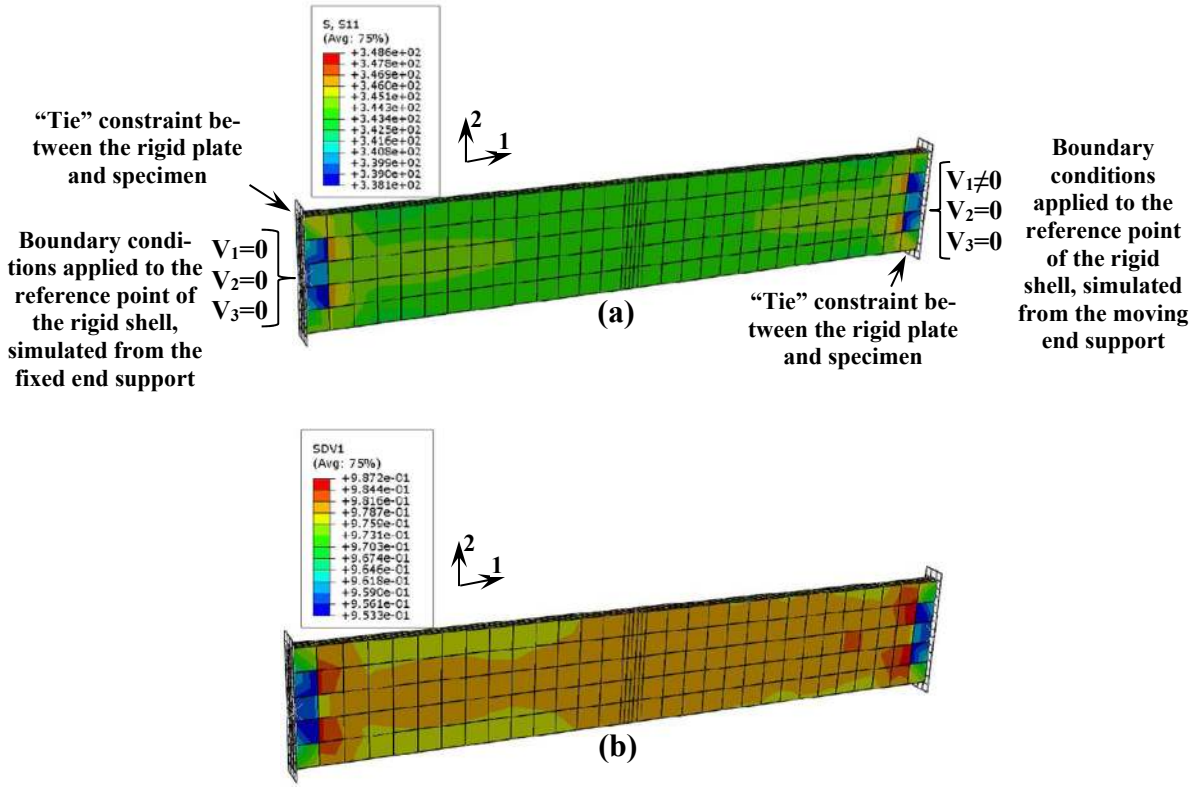

Figure 7: (a) Longitudinal stress distribution in the FE model of the ST-1 specimen prior to the rupture state, (b) Tensile fibers failure criteria (obtained by Equation (3)) at the same time.

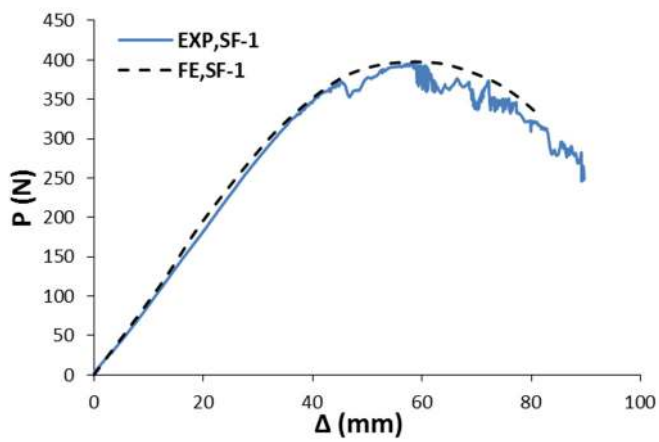

Figure 8: Load-deflection variations obtained by experiment and FE model for SF-1 specimen.

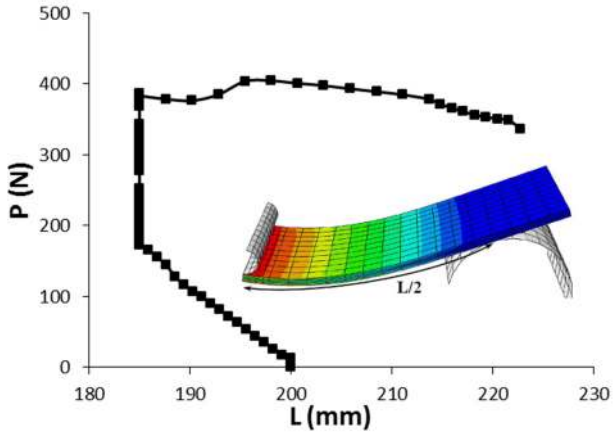

Figure 9: Variation of load versus the span length "L" measured for the SF-1 specimen.

The curved length of the beam span was measured by subtraction of the overhang length of the beam from the total length. Table 5 compares the elastic modulus and the ultimate strength measured for the bending UD specimens with those obtained for tensile specimens. Equation (1) gives the flexural modulus of the SF-1 specimen as E=13400 MPa. There is no doubt that the results, obtained by FE simulation of the composite beams, were more accurate than which were obtained by Equation (1). Based on the consistency of the FE modeling procedure, the load-deflection curve obtained by experiment was simulated by the FE model which showed that the most acceptable response of the beam was obtained when the flexural modulus was considered as E=13000 MPa (10% larger than the tensile modulus) through a try-and-error practice. The difference between the flexural moduli estimated by the numerical model and the analytical equation is attributed to the slippage of the beam on the support due to the large deflection and the non-ideal contact conditions which are not accounted for in the analytical formula (ASTM D790–07; 2007). It must be noted that the selection of a finer mesh did not make a significant influence on the accuracy of the flexural modulus estimated by the FE model.

Properties	Modulus of elasticity (MPa)			Ultimate strength (MPa)		
Specimens	Tensile modulus	Flexural modulus by Equation (1)	Flexural modulus by FE	Tensile strength	Flexural strength by Equation (2)	Flexural strength by FE
SF-1	11822	13400	13000	-	-	-
SF-2	11822	13600	13000	330	668	400
SF-3	1335	4440	4000	38	155	80

Table 5: Comparison of the mechanical properties obtained for the UD beam specimens by analytical formulas and FE models.

The L/D ratio of the SF-2 specimen was 33. Based on the load-deflection data depicted in Figure 10(a) and using Equation (1), the value of the flexural modulus for this case is determined as 13600 MPa , however, the FE results were in closer agreement with the experimental ones when the

flexural modulus of the beam was determined as E=13000 MPa. It is seen that by variation of the L/D ratio from 33 to 67 for the composite beams with UD 0°-plies, the flexural modulus remained almost constant. Smith et al. (1979) reported the flexural modulus of a kevlar 49/polyester composite beam with L/D ratio of 16, 35% lower than the modulus measured for a similar beam with L/D ratio of 60. The collapse load of SF-2 specimen occurred when a perpendicular crack in the tensile fibers appeared at the beam mid-span. The flexural strength, estimated by Equation (2), shows considerable discrepancy with the reality while this parameter can be estimated using FE numerical analysis to get more accurate results. Table 5 shows that the maximum experienced tensile stress at the outer tensile side of the beam is equal to 400 MPa (21% larger than the tensile strength of the specimen). By increasing the flexural modulus with respect to the tensile modulus and applying the strain-based failure criteria, a higher ultimate stress was estimated for the beams. Figure 11(a) shows the longitudinal stress (S_{11}) in SF-2 specimen prior to the failure state and Figure 11(b) shows the failed elements at the beam mid-span. This figure shows the boundary conditions which were applied for the beam models. The FE load-deflection curves (see Figure 10) show that if instead of strain-based failure criteria, the failure criteria was chosen based on the ultimate stresses (with the tensile strength of 330 MPa), the maximum peak load of this specimen would be considerably underestimated. Although the estimated ultimate load using the strain-based failure criteria is almost identical with the ultimate load measured in the experiment, the failure deflection estimated by the FE model is smaller than what is measured in the experiment. At the final part of the experimental load-deflection curve a slight softening region is observed prior to the failure point which is not accounted for in the FE model, so a larger failure deflection is observed in the experiment. Experimental observations showed that failure in the UD composite beams occurred in the whole tensile part of the beam cross-section, simultaneously. Around the cracked area, a delamination region was observed which will be discussed later on. Wisnom and Atkinson (1997) reported that the flexural failure of the UD carbon/epoxy laminates is usually a gradual process, with bundles of fibers breaking first at the surface and then progressively through the thickness.

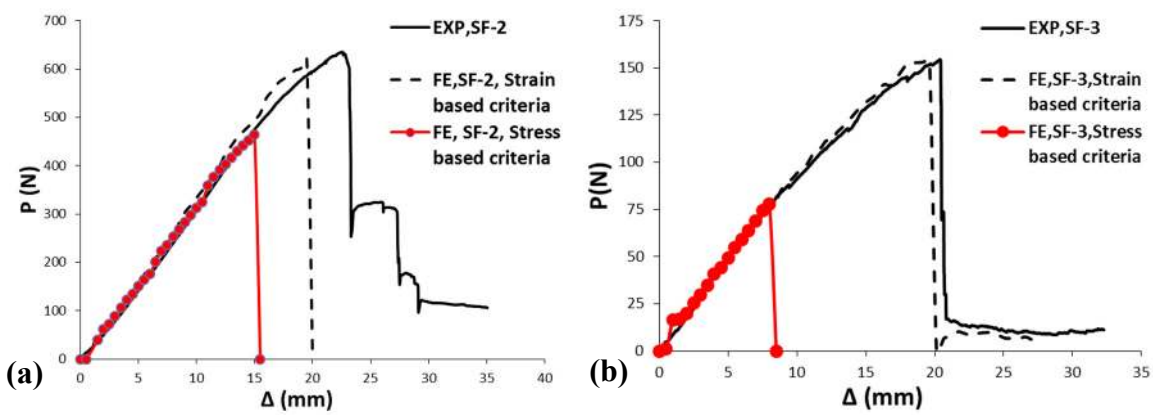

Figure 10: Comparison of the load-deflection curves obtained by experiment and FE models for (a) SF-2 and (b) SF-3.

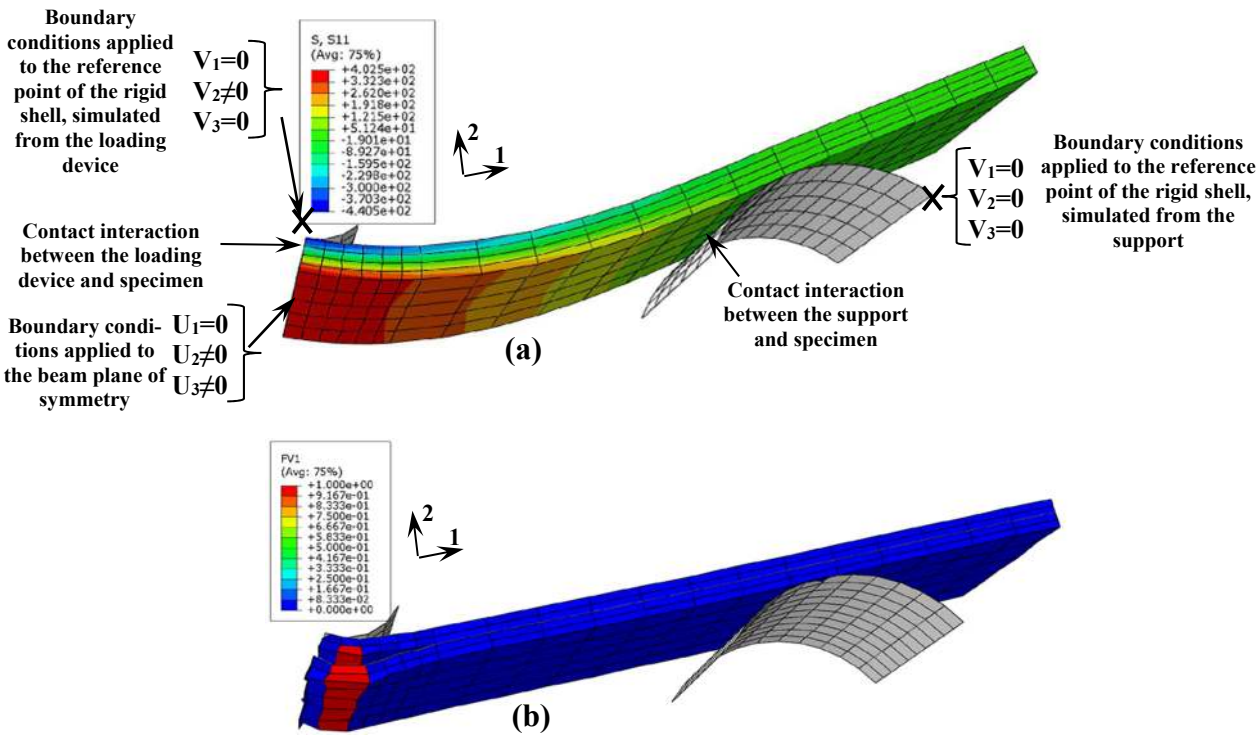

Figure 11: FE model of SF-2 specimen, (a) Longitudinal stress in the beam prior to cracking, (b) Fibers failure index in the beam after the collapse of the load-deflection curve.

Huang (2004) also conducted some experiments on the composite laminates made of knitted carbon fibers and reported a gradual flexural failure process under 4PB (four-point-bending) load. The load-deflection curves measured by Huang show a considerable softening behavior prior to the collapse load for UD specimens. Since in the present research the failure of the glass/vinyl ester beams was observed suddenly, it is concluded that the flexural failure for the laminate beams made of various composite materials may be different.

The load-deflection curves of the SF-3 specimen (with UD 90°-plies), obtained from the FE model and the experiment, were depicted in Figure 10(b). Table 4 shows that by Equation (1) the initial flexural modulus of the as E=4.44 GPa. The FE model-predicted this parameter as E=4 GPa. This experiment displayed a considerable increase of the flexural modulus relative to the tensile modulus for the laminate beam with UD-90° plies (about 250%) compared to the increase observed for the beam in the fibers direction. Roopa et al. (2014) also reported such an increase in the flexural modulus of the glass/vinyl ester laminates compared to the tensile modulus.

There are some researches in the literature which relate the difference between the tensile and flexural modulus to the different response of the material under tensile and compressive loads. Mujika et al. (2006) derived a formula to estimate the flexural modulus of the composite beams based on the difference of the elastic modulus of the material under tension and compression loads. According to this formula, if λ is the ratio of the elastic modulus under tension and compression loads

($\lambda=E_t/E_c$), and β is the ratio of the elastic modulus under bending over the tensile elastic modulus ($\beta=E_f/E_t$), the relation between these parameters is written as:

$$\beta = \frac{4}{(1+\sqrt{\lambda})^2} \tag{28}$$

For SF-3 specimen, the flexural and tensile moduli are considered as $(E_f)_0$=4000 MPa and $(E_t)_0$=1335 MPa, respectively, so by the aid of Equation (28), the compression modulus is obtained as $(E_c)_0$=39000 MPa which is not a reasonable value for the examined material. So, it seems that the mentioned hypothesis (difference of the tensile and compressive moduli) is not the only factor that justifies the difference of the flexural and the tensile moduli.

Collapse of the SF-3 specimen occurred due to a through the thickness crack. The FE results showed that the maximum stress, experienced on the tensile side of this beam, was 80 MPa, however, the pure tensile strength for the same material was measured as 38 MPa. By the considerable increase of the flexural modulus with respect to the tensile modulus, prediction of the flexural strength of SF-3 specimen using the stress-based failure criteria did not lead to an acceptable result. But the strain-based failure criteria gave accurate results. There was not any indication of delamination around the ruptured area for SF-3 specimen (see Figure 12), denoting lower inter-laminar stresses for this specimen.

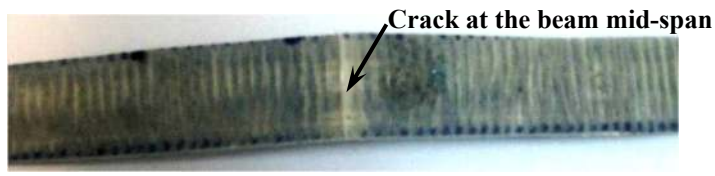

Figure 12: The tensile side of the SF-3 specimen after test shows no delamination.

4.2.2 Cross-Ply Laminates

Experimental observations about the UD laminate beams in the fibers and transverse directions indicated that the difference between the flexural and tensile moduli for the composite beams made of UD 0°-plies is negligible compared to the difference which is measured for the laminates made of UD 90°-plies. Therefore, for the beam specimens made of a combination of both 90° and 0°-plies, a variation of the flexural modulus is just attributed to the variation of the flexural modulus of the 90°-plies. For SF-4 and SF-5 specimens, the orientation of fibers in the top ply was different from that of the three bottom plies. The load-deflection curves, obtained from experiments and finite elements analyses are shown in Figure 13 for SF-4 and SF-5 specimens. The mesh convergence study showed that when the orientation of the fibers at the adjacent plies was different, each ply of the laminate must be discretized with at minimum two elements to consider the edge effect in the laminate. Based on the above assumptions, while the elastic modulus of the 0°-plies was assumed to be a constant value, equal to 13 GPa, by simulating the experimental curves the flexural modulus of the 90°-plies in the FE models of SF-4 and SF-5 specimens was estimated as 1.5 GPa and 2.2 GPa, respectively. The maximum load carrying capacity of SF-5 specimen reduced about 45% in

comparison to that of the SF-3 specimen. Due to the reduction of the thickness of the 90°-plies in SF-5 specimen, compared to that in the SF-3 specimen, the flexural modulus of the 90°-plies decreased about 35%. Using the strain-based failure criteria the maximum experienced stress in the 90°-plies was estimated equal to 45 MPa (18% larger than the strength measured in the associated tensile specimen).

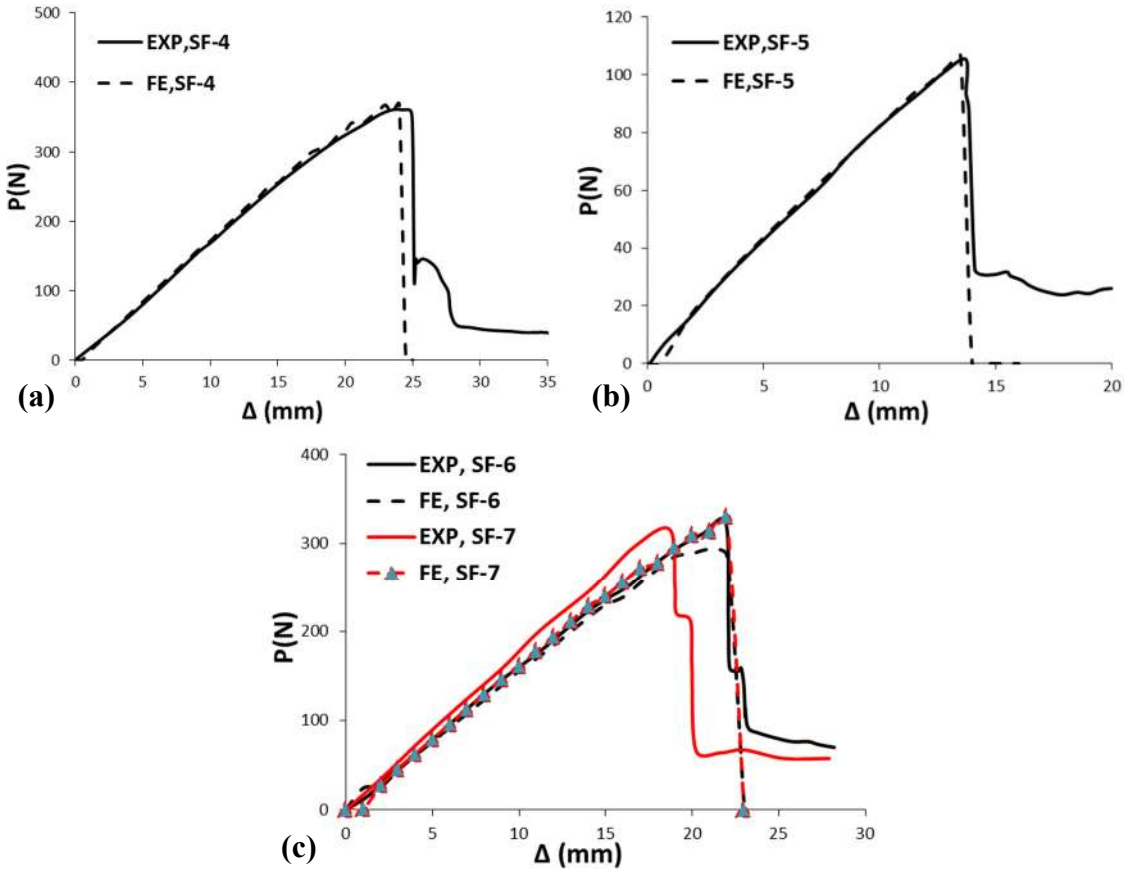

Figure 13: Load-deflection curves obtained by experiments and FE models for (a) SF-4, (b) SF-5, (c) SF-6 and SF-7 specimens.

The SF-6 and SF-7 specimens were cut from two perpendicular directions of an asymmetric cross-ply laminate. The load carrying capacity of these laminates was identical under tensile load, however, a larger flexural load carrying capacity was observed for the specimen which contains the 90°-plies closer to the tensile side of the beam (from top→0,90,0,90). The mid-span crack in these specimens penetrated through the whole thickness. In these specimens, there was not any delaminated area around the cracked region. The flexural modulus of the separate 90°-plies for the FE models of both specimens was determined as 1.5 GPa. Figure 13 shows the validity of the obtained FE results. The experimental specimen. Examination of these specimens showed that the flexural modulus of the 90°-plies does not increase by an increase in the number of the separate 90°-plies while by an increase in the number of the adjacent 90°-plies, the flexural modulus of these layers

increases considerably. The results, obtained from the finite elements analyses, showed that failure of both SF-6 and SF-7 specimens are controlled by the failure of the 0 ° -plies. Figure 14 shows an outcome of all observations about the variation of the flexural modulus of 90 ° -plies versus the thickness (number) of the adjacent 90 ° -plies for various layups of the composite beams, examined in the experiments. This figure shows that variation of the results show that the flexural modulus of the SF-7 specimen is slightly higher than that of the SF-6 flexural modulus does not have a linear trend. The results, obtained by progressive failure analyses for all specimens, showed that by estimation of the flexural modulus of the composite beams and using the strain-based failure criteria, one can achieve acceptable prediction about the maximum load carrying capacity of the beams with various layups.

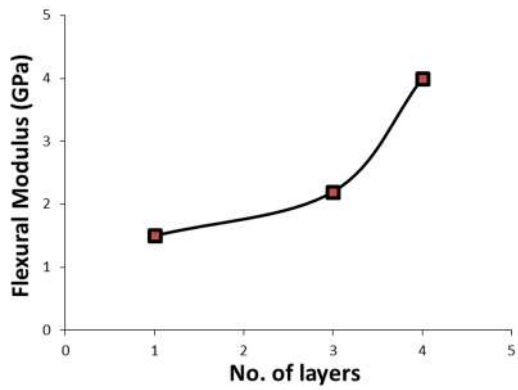

Figure 14: Variation of the flexural modulus of 90 ° -plies by variation of the thickness of the adjacent 90 ° -plies observed in the various specimens.

4.3 Influence of Delamination on the Flexural Failure

Physical observation of SF-2 specimen showed a delaminated area near the ruptured region of the beam (see Figure 15(a)). The occurrences of delamination in the UD composite beams was also reported by Wisnom and Atkinson (1997) which was simulated by Li et al. (2013) using cohesive zone elements. Ullah et al. (2012) also used cohesive elements to simulate delamination of the bending CFRP laminates. In the experiments examined in the present research, the delamination occurred at the stage of the final failure of the beam. In the present research, the capability of delamination feature was included in the finite element analysis of the SF-2 specimen to estimate the effect of delamination on the load carrying capacity of the beam. Simulation of delamination using VCCT is seen in Figure 15(b). "CSDMG" index in this figure denotes the G_{equiv}/G_{equivC} ratio presented in Equation (27). When this value becomes unity it indicates debonding between the contacted nodes in the adjacent layers. The finite element results showed that no delamination is observed prior to the fibers rupture. Actually, in the experimental observation, the delamination was detected between the ruptured tensile and compressive layers, so it seems that the reason for delamination was referred to the breakage of the tensile fibers. This description indicates that although inter-laminar damage was observed in the ultimate state of the composite beams it was occurred in following of the tensile failure of the fibers. Therefore, the delamination does not have considerable influence on

the failure of the composite beams. Figure 16 shows a variation of SERRs in the mentioned modes of inter-laminar failure at node "i" shown in Figure 15(b) versus the beam mid-span deflection. These curves indicate the occurrence of delamination due to the second fracture mode (sliding). The delaminated area in the other specimens was ignorable.

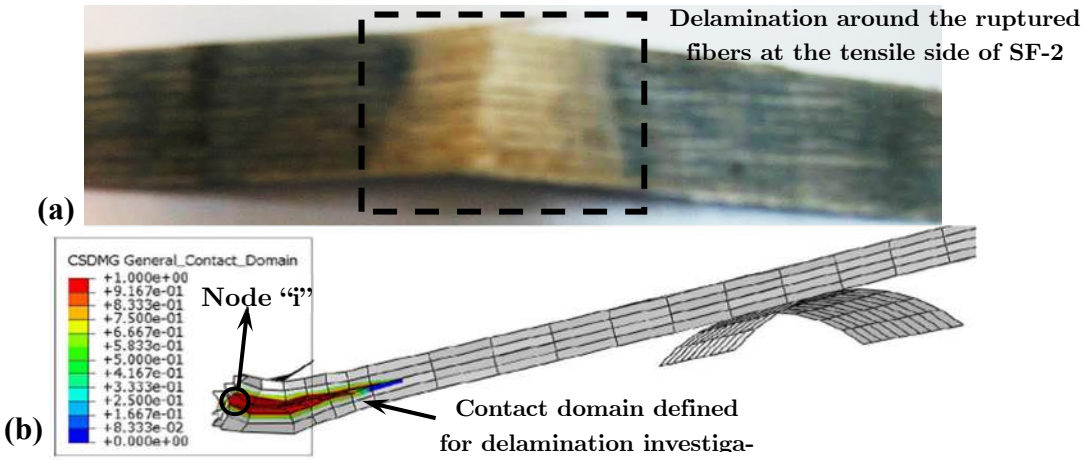

Figure 15: (a) Backside of the SF-2 specimen shows delamination around the ruptured fibers, (b) Delamination simulated in the FE model.

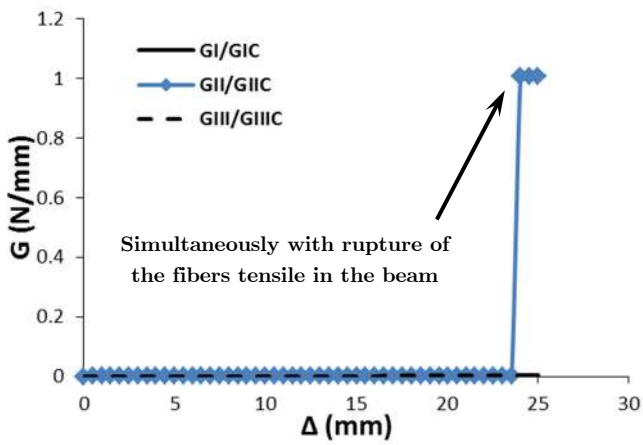

Figure 16: Variation of SERRs in three modes of inter-laminar failure at node "i" (shown in Figure 15(b)) versus the beam mid-span deflection.

5 CONCLUSIONS

In this paper, the variation of the flexural modulus in the composite beams was investigated for various layup methods of the laminates by the aid of the experiments and finite element analyses. It was shown that the damage occurrence in the polymeric part of the composite materials is mainly responsible for the nonlinear behavior of the beams. Variation of the elastic modulus in the compo-

site beams was mainly attributed to the nonlinear response of the 90°-plies in the laminates. The first step of the experimental program consisted of tensile tests which yielded the stress-strain response of the laminates under tensile tests. The same data were exploited for verification of the developed progressive damage analysis procedure. The flexural behavior of the composite beams was examined by conducting of the 3PB experiments. For simulation of the flexural failure mechanism, both intra-laminar and inter-laminar damage modes were included in the FE models. Prediction of the intralaminar damage was carried out based on the CDM theory while the inter-laminar damage (delamination) was simulated using VCCT. The obtained results showed that the progressive damage analyses with consideration of the strain-based failure criteria could predict the flexural strength of the composite beams accurately. The strain-based failure criteria indicated that due to the growth of the elastic modulus of the laminates under bending load, the measured ultimate stress in the composite beams increases relative to the tensile strength. The flexural modulus of the laminates was observed dependent on the layup method of the laminates. Simulation of the composite beams by FE models showed that the flexural modulus of the 0°-plies in the various laminate beam specimens remained almost constant, however, when the number of the adjacent 90°-plies increased in a laminate, the flexural modulus of these plies improved considerably. Of course, by increasing the number of the separate 90°-plies in the beam specimens, little growth was seen in the flexural modulus (the great enhancing influence was observed due to the presence of the adjacent 90°-plies). At the ultimate state of the composite beams, delamination damage was observed for the specimen with UD 0°-plies simultaneously with rupture of the tensile fibers of the beam and therefore it did not have a considerable influence on the ultimate strength of the composite beams.

References

ABAQUS/Analysis user's manual. (2010). Version 6.10, ABAQUS Inc.

Batra, R.C., Gopinath, G., Zheng, J.Q. (2012). Damage and failure in low energy impact of fiber-reinforced polymeric composite laminates. Composite Structures 94: 540–7.

Bažant, Z.P. Oh, B.H. (1983). Crack band theory for fracture of concrete. Materials and Structures 16: 155–77.

Bullock, R.E. (1974). Strength ratios of composite materials in flexure and in tension. J. Composite Materials 8: 200-6.

Camanho, P.P., Davila, C.G. (2002). Mixed-mode decohesion finite elements for the simulation of delamination in composite materials. NASA/TM-2002-211737.

Cattell, M.K., Kibble, K.A., (2001). Determination of the relationship between strength and test method for glass fibre epoxy composite coupons using Weibull analysis. Materials and Design 22: 245-50.

Doudican, B.M., Zand, B., Amaya, P., et al. (2012). Strain energy based failure criterion: comparison of numerical predictions and experimental observations for symmetric composite laminates subjected to triaxial loading. J. Composite Materials 47(6–7): 847–66.

Echaabi, J., Trochu, F., Pham, X.T., et al. (1996). Theoretical and experimental investigation of failure and damage progression of graphite-epoxy composites in flexural bending test. J. Reinforced Plastics and Composites 15: 740–55.

Garnich, M.R., Akula, V.M.K., (2009). Review of degradation models for progressive failure analysis of fiber reinforced polymer composites. Applied Mechanics Reviews 62: 1-33.

Hashin, Z. (1965). On elastic behaviour of fibers reinforced materials of arbitrary transverse phase geometry. J. Mechanics and Physics of Solids 13, 119–34.

Hashin, Z., Rotem, A., (1973). A fatigue criterion for fiber-reinforced materials. J. Composite Materials 7: 448–64.

Huang, Z.M. (2004) Progressive flexural failure analysis of laminated composites with knitted fabric reinforcement. Mechanics of Materials 36: 239-60.

Jones, R.M. (1978). Mechanics of Composite Materials with different moduli in tension and compression. Final scientific report, Air force office of scientific research.

Jones, R.M. (1999). Mechanics of composite materials, Philadelphia: Taylor and Francis Inc.

Kachanov, L.M. (1958). On the creep fracture time. Izv Akad Nauk USSR Otd Tekh 8, 26–31. (In Russian)

Krueger, R. (2002). The virtual crack closure technique: history, approach and applications. NASA/CR-2000-ICASE Report No.2002-211628.

Lade`veze, P., Lubineau, G. (2002). An enhanced mesomodel for laminates based on micromechanics. Composites Science and Technology 62: 533–41.

Lapczyk, I., Hurtado, J.A. (2007). Progressive damage modeling in fiber-reinforced materials. Composites Part A-Appls, 38: 2333–41.

Li, X., Hallett, S.R., Wisnom, M.R. (2013). A finite element based statistical model for progressive tensile fibre failure in composite laminates. Composites B Engineering 45; 433–9.

Maimi, P., Camanho, P.P., Mayugo J., et al. (2006). A thermodynamically consistent damage model for advanced composites. NASA/TM-2006-214282.

Maimi, P., Camanho, P.P., Mayugo, J.A., et al. (2007). A continuum damage model for composite laminates: Part I – constitutive model. Mech. Mater. 39: 897–908.

Meng, M., Le, H.R., Rizvi, M.J., Grove, S.M. (2015). The effects of unequal compressive/tensile moduli of composites. Composite Structures doi: http://dx.doi.org/10.1016/j.compstruct.2015.02.064.

Mines, R.A.W., Alias, A. (2002). Numerical simulation of the progressive collapse of polymer composite sandwich beams under static loading. Composites Part A-Appls 33: 11–26.

Moreno, M.C.S., Gutiérrez, A.R., Vicente, J.L.M. (2016) Different response under tension and compression of unidirectional carbon fibre laminates in a three-point bending test. Composite Structures 136: 706-11.

Mujika, F., Carbajal, N., Arrese, A., Mondragon, I. (2006) Determination of tensile and compressive moduli by flexural tests. Polymer Testing 25, 766–71.

Nazari, A.R. (2016) Investigation of load carrying and progressive failure in the composite sandwich panels with elastomeric foam core under biaxial bending. PhD Thesis, Amirkabir University of Technology, Iran. (In persian)

Nazari, A.R., Hosseini-Toudeshky, H., Kabir, M.Z. (2017) Experimental investigations on the sandwich composite beams and panels with elastomeric foam core. Journal of Sandwich Structures and Materials Accepted for publication.

Nazari, A.R., Kabir, M.Z., Hosseini-Toudeshky, H. (2017) Investigation of elastomeric foam response applied as core for composite sandwich beams through progressive failure of the beams. Journal of Sandwich Structures and Materials DOI: 10.1177/1099636217697496.

Ochoa, O., Reddy, J.N. (1992). Finite Element Analysis of Composite Laminates. Dordrecht: Kluwer Academic Publishers.

Roopa, T.S., Murthy, H.N., Sudarshan, K., et al. (2014). Mechanical properties of vinylester/glass and polyester/glass composites fabricated by resin transfer molding and hand lay-up. J. Vinyl Additive and Technology doi: 11.1002/vnl.21393.

Rybicki, E.F., Kanninen, M.F. (1977). A finite element calculation of stress intensity factors by a modified crack closure integral. Engineering Fracture Mechanics 9: 931-38.

Sadeghi, G., Hosseini-Toudeshky, H., Mohammadi, B. (2014). An investigation of matrix cracking damage evolution in composite laminates-Development of an advanced numerical tool. Composite Structures 108: 937-50.

Smith, D.L., Wardle, M.W., Zweben, C. (1979). Test methods for fiber tensile strength, composite flexural modulus and properties of fabric-reinforced laminates. In: SW Tsai (ed) Composite materials: testing and design (Fifth Conference), ASTM STP 674. West Conshohocken: American society for testing and materials, pp. 228-62.

Smith, P.A., Ogin, S.L. (1999). On transverse matrix cracking in cross-ply laminates loaded in simple bending. Composites Part A-Appls 30: 1003–8.

Soden, P.D., Hinton, M.J., Kaddour, A.S. (1998). A comparison of the predictive capabilities of current failure theories for composite laminates. Composites Science and Technology 58: 1225-54.

Soden, P.D., Hinton, M.J., Kaddour, A.S. (1998). Lamina properties, lay-up configurations and loading conditions for a range of fiber-reinforced composite laminates. Composites Science and Technology 58: 1011–22.

Standard test methods for flexural properties of unreinforced and reinforced plastics and electrical insulating materials. (2007). ASTM, Designation: D790–07.

Timoshenko, S.P., Gere, J.M., (1972). Mechanics of Materials. NewYork: Van Nostrand Reinhold Co.

Tolf, G., Clarin, P. (1984) Comparison between flexural and tensile modulus of fibre composites. Fibre Science and Technology 21: 319-26.

Ullah, H., Harland, A.R., Lucas, T., et al. (2012). Finite-element modelling of bending of CFRP laminates: Multiple delaminations. Computational Materials Science 52: 147–56.

Whitney, J.M. Knight, M. (1980). The relationship between tensile strength and flexure strength in fiber-reinforced composites. Experiental Mechanics 20(6): 211-6.

Wisnom, M.R. (1992). The relationship between tensile and flexural strength of unidirectional composites. J. Composite Materials 26: 1173-80.

Wisnom, M.R. Atkinson, J.W. (1997). Reduction in tensile and flexural strength of unidirectional glass fibre–epoxy with increasing specimen size. Composite Structures 38(1–4): 405–11.

Wolfe, W.E., Butalia, T.S. (1998). A strain-energy based failure criterion for non-linear analysis of composite laminates subjected to biaxial loading. Composites Science and Technology 58: 1107-24.

Wu, E.M., Reuter Jr. R.C. (1965). Crack extension in fiberglass reinforced plastics. University of Illinois, Champaign.

Zweben, C. (1994). Is there a size effect in composite materials and structures? Composites 25: 451-4.

APPENDIX A

The non-zero components of C_d matrix are derived as:

$$M_{11} = \frac{E_1}{D}.(1-d_f).[1-\nu_{23}\nu_{32}.(1-d_m)^2] \tag{A.1}$$

$$M_{12} = \frac{E_1}{D}.(1-d_f).(1-d_m).[\nu_{21}+\nu_{23}\nu_{31}(1-d_m)] \tag{A.2}$$

$$M_{13} = \frac{E_1}{D}.(1-d_f).(1-d_m).[\nu_{31}+\nu_{21}\nu_{32}(1-d_m)] \tag{A.3}$$

$$M_{21} = \frac{E_2}{D}.(1-d_f).(1-d_m).[\nu_{12}+\nu_{13}\nu_{32}(1-d_m)] \tag{A.4}$$

$$M_{22} = \frac{E_2}{D}.(1-d_m).[\nu_{13}\nu_{31}(d_f+d_m-d_f d_m-1)+1] \tag{A.5}$$

$$M_{23} = \frac{E_2}{D}.(1-d_m)^2.[\nu_{32} + \nu_{12}\nu_{31}(1-d_f)] \tag{A.6}$$

$$M_{31} = \frac{E_3}{D}.(1-d_f).(1-d_m).[\nu_{13} + \nu_{12}\nu_{23}(1-d_m)] \tag{A.7}$$

$$M_{32} = \frac{E_3}{D}.(1-d_m)^2.[\nu_{23} + \nu_{13}\nu_{21}(1-d_f)] \tag{A.8}$$

$$M_{33} = \frac{E_3}{D}.(1-d_m).[\nu_{12}\nu_{21}(d_f + d_m - d_f d_m - 1) + 1] \tag{A.9}$$

$$M_{44} = \frac{(1-d_s^l)}{G_{12}}, M_{55} = \frac{(1-d_s^l)}{G_{13}}, M_{66} = \frac{(1-d_s^t)}{G_{23}} \tag{A.10}$$

$$D = 1-(1-d_f)(1-d_m)(\nu_{12}\nu_{21}+\nu_{13}\nu_{31}) - \nu_{23}\nu_{32}(1-d_m)^2 - (1-d_f)(1-d_m)^2(\nu_{12}\nu_{23}\nu_{31}+\nu_{13}\nu_{32}\nu_{21}) \tag{A.11}$$